ACS APPLIED MATERIALS & INTERFACES

Research Article

www.acsami.org

Nano Copper Oxide-Incorporated Mesoporous Carbon Composite as Multimode Adsorbent for Selective Isolation of Hemoglobin

Yang Zhang,[†] Li-Gang Xing,[†] Xu-Wei Chen,*[,†] and Jian-Hua Wang*[,†,‡]

[†]Research Center for Analytical Sciences, Northeastern University, Box 332, Shenyang 110819, China

[‡]Collaborative Innovation Center of Chemical Science and Engineering, Tianjin 300071, China

Supporting Information

ABSTRACT: Assembly of nano-objects with tunable size, morphology and function into integrated nanostructures is critical for the development of a novel nanosystem in adsorption, sensing and drug/gene delivery. We demonstrate herein the fabrication of ordered mesoporous carbon by assembling uniform and highly dispersed copper-oxide (Cu_xO_y) nanoparticles into the mesopores via evaporation of solvent from the mixture of triblock copolymer, carbon source and metal nitrate hydrate. The ordered 2D hexagonal mesoporous carbon composite possesses a large surface area of 580.8 cm^2/g, a uniform pore size of 5.4 nm, a large pore volume of 0.64 cm^3/g and a high metal content of 3.32 wt %. The mesoporous composite exhibits excellent adsorption selectivity and high adsorption capacity to hemoglobin (Hb) under the synergistic effect of hydrophobic and metal-affinity interactions as well as size exclusion. This facilitates multimode adsorption of hemoglobin fitting Langmuir adsorption model and offers an adsorption capacity of 1666.7 mg g^{-1} for hemoglobin. The mesoporous composite is used for the isolation of hemoglobin from human whole blood with high purity. It demonstrates the potential of the copper-oxide nanoparticle-embedded mesoporous carbon composite in selective isolation/removal of specific protein species from biological sample matrixes.

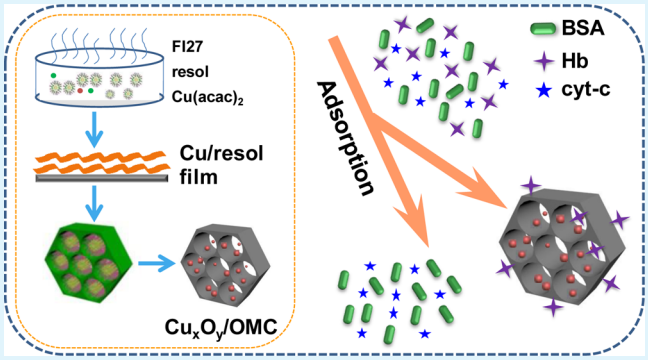

KEYWORDS: *mesoporous carbon, copper-oxide nanoparticles, hemoglobin, multimodal adsorption*

INTRODUCTION

The progress of proteomics has attracted considerable interest in the development of efficient separation/purification approaches for proteins allowing for the direct isolation of specific protein species from complex biological systems. Immobilized metal-affinity separation has been recognized as a powerful technique for protein purification ever since its commencement.[1] As an illustration, immobilized metal-affinity chromatography (IMAC) offers an excellent platform for the purification of specific proteins based on the coordination reactions between the metal−chelate complexes from affinity matrixes and electron donor groups from specific amino acids accessible on biomolecules.[2] However, such systems for protein isolation are generally characterized by complicated operation and high cost. The multiple modifications involved in the whole process are time-consuming and significantly discount the purification efficiency in large scale practices or commercial applications.

Carbon based materials,[3−6] metal- or metal-oxide-containing carbon materials have been widely used as adsorbents, catalysts, drug delivery carriers and electrodes. Typically, they are fabricated by incorporating metals or metal oxides within the pores via impregnation or modification of metal/metal-oxide nanoparticles onto the carbon mesopore walls.[7−9] This strategy exhibits the superiority in confining the growth of nanoparticles within the pores and it is widely adopted to control particle sizes.[10,11] As a kind of intriguing porous material, ordered mesoporous carbons (OMCs) have attracted considerable attention due to the merits of continuous channels, controllable pore structure, uniform pore size (2−50 nm) and large pore volume for supporting metal nanoparticles.[12−15]Titanium carbide nanoparticle-containing mesoporous carbon has been prepared by using a facile approach with coassembly of titanium citrate, phenolic resol and triblock-copolymer F127.[16] Ir-incorporated OMC is found to exhibit high activity for the catalytic decomposition of N_2H_4. In general, metal particles of larger size, e.g., ≥30 nm, are always embedded into the pores in order to achieve a high metal loading content. Meanwhile, the incorporation of large-size particles will inevitably lead to congestion of the mesopores and thus cause limitation on mass-transfer.[17] In this respect, it is highly desirable to incorporate smaller nanoparticles into the mesoporous frameworks to maintain the open pore structure and, in the meantime, to improve the activity.

In the present study, we report a chelate-assisted coassembly approach for the preparation of ordered mesoporous carbon

Received: October 16, 2014
Accepted: February 18, 2015
Published: February 18, 2015

DOI: 10.1021/am508836m
ACS Appl. Mater. Interfaces 2015, 7, 5116−5123

Scheme 1. Schematic Illustration of the Preparation of Cu_xO_y Nanoparticle-Incorporated Mesoporous Carbon Frameworks via Solvent Evaporation Induced Coassembly

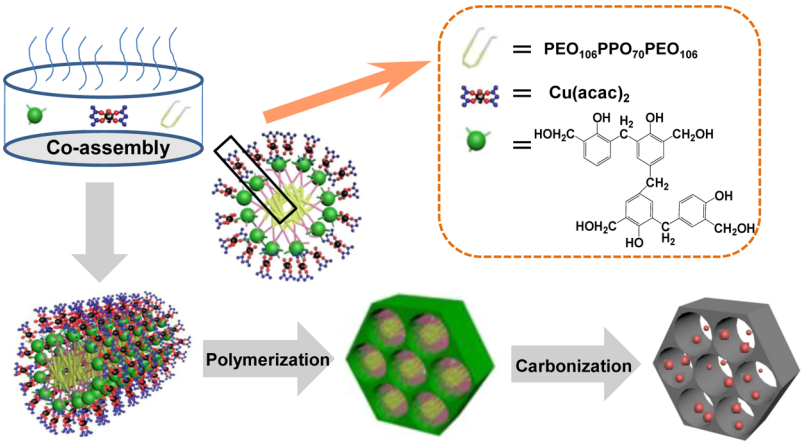

embedded with copper-oxide nanoparticles (Cu_xO_y/OMC). The Cu_xO_y/OMC nanocomposite is merited with 2D hexagonal mesoporos structure and a uniform pore size in addition to a high surface area. The in situ grown Cu_xO_y nanoparticles are uniform and highly dispersed inside the ordered mesopores with 3.32 wt % Cu. As a novel adsorbent, the Cu_xO_y/OMC composite exhibits high selectivity for the adsorption of hemoglobin due to the OMC−protein hydrophobic interaction, the specific metal-affinity interaction between Cu_xO_y nanoparticles and histidine residues of protein species, and size-exclusion effect of the mesopores. The multiple interactions between Cu_xO_y/OMC composite and protein species offer great potential for the development of multimode adsorption strategy for the isolation/purification of hemoglobin from complex matrices with the merits of high adsorption capacity and favorable selectivity.

EXPERIMENTAL SECTION

Chemicals and Apparatus. Poly(ethylene oxide)-*block*-poly(propylene oxide)-*block*-poly(ethylene oxide) triblock copolymer Pluronic F127 ($PEO_{106}PPO_{70}PEO_{106}$, Mw = 12 600), formalin solution (37 wt %), hemoglobin (Hb, H2625, 95%), bovine serum albumin (BSA, A 3311, >98%), cytochrome c (cyt-c, 30398, >95%), tris(hydroxymethyl)aminomethane (Tris, T1378, >99.9%), glycine and histidine were purchased from Sigma-Aldrich (St. Louis, USA). $Cu(NO_3)_2{\cdot}3H_2O$, phenol, acetylacetone (acac), ethanol, hydrochloric acid, nitric acid, hydrogen peroxide, carbonate, phosphate and citrate were purchased from Sinopharm Chemical Reagent Co. Ltd. (Shanghai, China). These reagents were at least of analytical-reagent grade and used as received without any further treatment.

The protein molecular weight marker (Low, D530AJ, Takara Biotechnology Company, Dalian, China) is a mixture of six purified proteins (M_r in kDa: phosphorylase B, 97.2; serum albumin, 66.4; ovalbumin, 44.3; carbonic anhydrase, 29.0; trypsin inhibitor, 20.1; lysozyme, 14.3). Human blood sample from a healthy volunteer is provided by the Hospital of Northeastern University.

Small-angle X-ray scattering (SAXS) measurement is performed on a Nanostar U SAXS system (Bruker, Germany) using Cu Kα radiation (40 kV, 35 mA). The *d*-spacing values are calculated by the formula of $d = 2\pi/q$. X-ray diffraction (XRD) patterns are recorded using an X'Pert Pro MPD X-ray diffractometer (PW3040/60, PANalytical BV, Holland) with Cu Kα irradiation. Nitrogen sorption/desorption isotherm is measured at 77 K with a Micromeritcs Tristar 3000 analyzer (USA). Before the sorption/desorption measurement, the samples are degassed in a vacuum at 200 °C for 10 h. The Brunauer−Emmett−Teller (BET) method is used to calculate the specific surface area according to the adsorption data in a relative pressure range from 0.05 to 0.25. The pore size distribution (PSD) is calculated based on the adsorption branch by using the Barrett−Joyner−Halenda (BJH) model. High-resolution transmission electron microscopy (HR-TEM) images are recorded on a JEM-2100 F microscope (JEOL, Japan) operated at 200 kV. The mesoporous samples are suspended in ethanol and transferred onto a microgrid for HR-TEM measurements. X-ray photoelectron spectroscopy (XPS) scanning curve of the Cu_xO_y/OMC composite is obtained on an ESCALAB 250 surface analysis system (Thermo Electron, England) with an Al Kα 280 eV excitation source. Thermogravimetric analysis (TGA) is performed on a TGA 290C analyzer (Netzsch Company, Germany) at a heating rate of 10 °C min^{-1} under oxygen atmosphere. A PB-10 pH Meter (Beijing Sartorius Instruments Co., Ltd., China) is used for pH measurement. The quantification of Cu in the Cu_xO_y/OMC composites is performed by using inductively coupled plasma mass spectrometry (ICP-MS, Agilent 7500, Agilent Technologies) instrument with a cross-flow nebulizer, Scott-type spray chamber, and a 2.0 mm (i.d.) alumina injector.

Preparation of the Cu_xO_y/OMC Composite. Soluble resol (phenol/formaldehyde) precursors are first prepared via a base-catalyzed procedure as reported previously[18] and described shortly in the following: 5.0 g of phenol is heated to melt at 45 °C and 1.06 g of NaOH solution (20 wt %) is then added slowly under stirring; 8.8 g of formaldehyde (37 wt %) is subsequently added dropwise, and the obtained mixture is heated at 70 °C under stirring for 90 min. After the mixture is cooled down to room temperature, it is adjusted to pH 6−7 by using 2.0 M HCl. The produced NaCl and water are removed by centrifugation and vacuum distillation, respectively. The obtained resol precursor is redissolved in ethanol (20 wt %) for future use.

Copper-oxide nanoparticles embedded mesoporous carbon is prepared according to a chelate-assisted coassembly strategy.[19,20] The preparation is accomplished by gently evaporation of an ethanol solution containing Pluronic F127, resol, acetylacetone and copper nitrate hydrate. In general, 1.0 g of Pluronic F127 is dissolved into 14.0 g of absolute ethanol; then 5.0 g of resol precursor solution is added, and the mixture is stirred for 10 min. 0.097 g of $Cu(NO_3)_2{\cdot}3H_2O$ dissolved in 3.5 g of ethanol and various amounts of acetylacetone (0, 0.03, 0.045, and 0.06 g, 0−60 wt % relative to the hydrated metal nitrite) is sequentially added dropwise into the above mixture. After the mixture is stirred for 30 min, it is cast onto a Petri dish, followed by evaporation of ethanol at room temperature for 12 h. Then the generated sticky films are heated at 100 °C for 24 h. Afterward, the composite films are scrapped off and ground into powders, followed by calcination in a tube furnace at 600 °C for 3 h at a temperature ramp of 1 °C min^{-1} under N_2 atmosphere. During the carbonization of resol precursor in the calcination process, Cu_xO_y nanocrystallites are generated in situ. The contents of copper are quantified with ICP-MS by digesting the composites in a microwave digestion system with HNO_3 and H_2O_2 at a volume ratio of 2:1 to ensure complete

DOI: 10.1021/am508836m
ACS Appl. Mater. Interfaces 2015, 7, 5116−5123

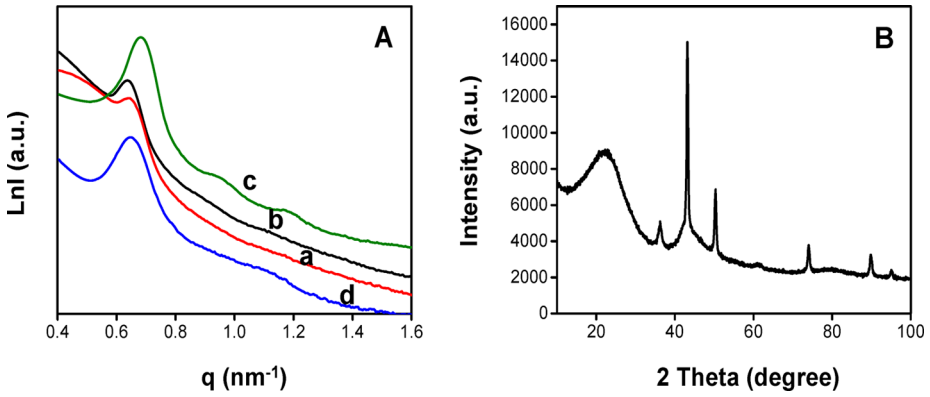

Figure 1. (A) SAXS of the Cu_xO_y/OMC composite with copper contents of 0.49, 2.12, 3.32 and 5.56 wt % prepared in the presence of 0.0, 0.03, 0.045 and 0.06 g of acac; (B) wide-angle XRD patterns of the Cu_xO_y/OMC composite.

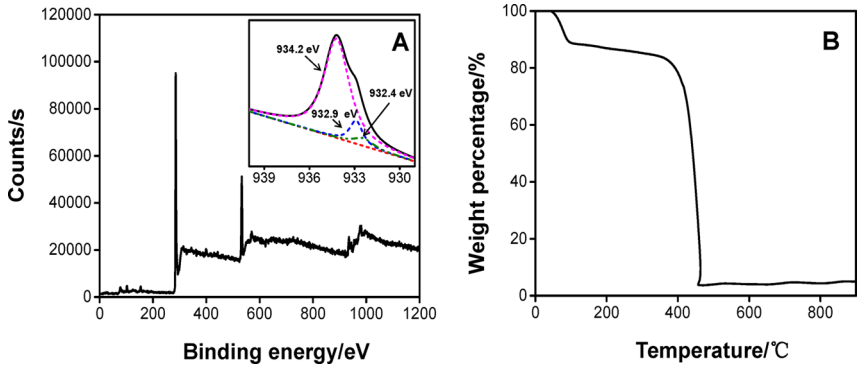

Figure 2. XPS (A) and TGA (B) analysis results for the Cu_xO_y/OMC composite.

dissolution of copper. For the sake of comparison, the preparation of bare OMC without metallic nanoparticles follows a similar procedure in the absence of $Cu(NO_3)_2{\cdot}3H_2O$.

Protein Adsorption. To investigate the performance of the as-prepared Cu_xO_y/OMC composite on the adsorption of protein species, three proteins with different hydrodynamic size, structure and isoelectric point (pI), i.e., bovine serum albumin (BSA, Mw = 66 400 Da, ~10 nm, pI 4.9), hemoglobin (Hb, Mw = 15 500 Da, ~5.0 nm, pI 6.8–7.0) and cytochrome c (cyt-c, Mw = 13 750 Da, ~3.0 nm, pI 9.8–10.1), are employed as model guest molecules for investigating the adsorption behaviors of the composite. The adsorption of these proteins of same concentrations is carried out at various pH values. pH value of the medium is regulated by a 4.0 mmol L^{-1} Britton–Robinson (BR) buffer within a range of pH 4–11.

Generally, 2.0 mg of the Cu_xO_y/OMC composite is mixed with 1.0 mL of protein solution. The mixture is shaken at room temperature for 30 min to facilitate protein adsorption. The reaction mixture is gently centrifuged at 3000 rpm for 4 min, and the supernatant is collected to quantify the residual proteins in the original solution by monitoring the soret absorbance at 409 nm for cyt-c and 405 nm for Hb, respectively. BSA is stained by Coomassie brilliant blue and measured at 595 nm.[15,21,22] After the adsorption process, the Cu_xO_y/OMC composite is prewashed with 1.0 mL of distilled water to remove any loosely retained species on the adsorbent surface. Thereafter, 1.0 mL of eluent (0.5 wt % SDS) is added and the mixture is then oscillated for 40 min to facilitate the recovery of adsorbed proteins from the surface of the Cu_xO_y/OMC composite. The supernatant containing the recovered protein species is finally collected by centrifugation at 3000 rpm for 4 min for the ensuing investigations.

RESULTS AND DISCUSSION

Preparation and Characterization of the Cu_xO_y/OMC Composite. The preparation of ordered mesoporous carbon embedding with Cu_xO_y nanoparticles is illustrated in Scheme 1. This is a chelate-assisted solvent evaporation induced coassembly strategy, with amphiphilic triblock copolymer as the template, soluble low-molecular weight polymer of phenol and formaldehyde resol as the carbon source, copper nitrate as the metallic source and acetylacetone as the coupling reagent.

In an ethanol solution containing the F127 template, resol and $Cu(NO_3)_2{\cdot}3H_2O$, hydrogen bond is formed between phenolic hydroxyl groups of resol molecules and EO segments of Pluronic F127 template, and the coordination of phenol with Cu^{2+} produces an emerald copper–phenol complex.[23] Meanwhile, the chelation between Cu^{2+} and acetylacetone contributes to in situ growth of metallic nanoparticles with semiexposed morphology. As a coupling reagent, acetylacetone itself is also involved in the coassembly process. A large dosage of acetylacetone helps to confine the growth of metallic crystals by effectively coordinating with copper and retarding its hydrolysis during the coassembly. After accomplishing these reactions, the ethanol solution is cast onto a Petri dish to evaporate continuously and form a thin film therein, in which the amphiphilic F127 associated with resol and Cu^{2+} assembled into a highly ordered mesostructure. Afterward, the decomposition of F127 template during the pyrolysis at 600 °C results in the formation of highly ordered and aligned mesopores, and meanwhile, the phenolic resin framework is carbonized into mesoporous carbon accompanied by in situ growth of Cu_xO_y nanoparticles.

SAXS patterns of four Cu_xO_y/OMC composites (Figure 1A) show similar three well resolved scattering peaks at q values of 0.60, 0.97 and 1.18 nm^{-1}, referring to the 10, 11 and 20 reflections of 2D hexagonal mesostructure. Meanwhile, it illustrates the analogous long-range pore structures of Cu_xO_y/

DOI: 10.1021/am508836m
ACS Appl. Mater. Interfaces 2015, 7, 5116–5123

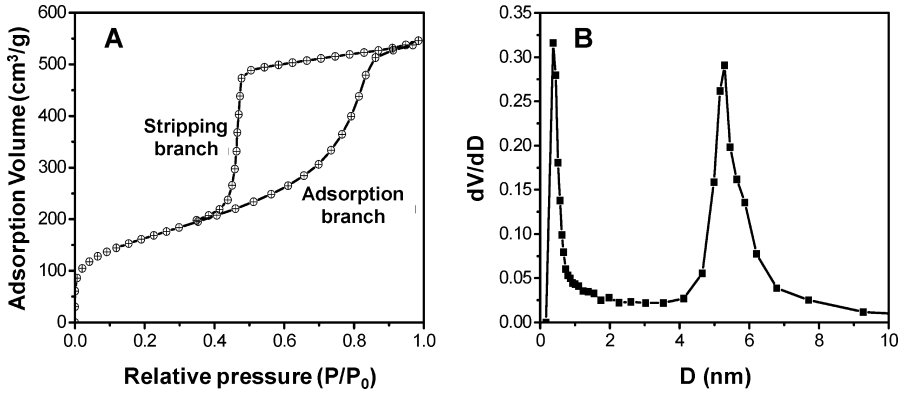

Figure 3. N_2 sorption/desorption isotherms (A) and the corresponding pore size distribution curve (B) of the Cu_xO_y/OMC composite.

OMC containing various amount of copper. The decrease of acac from 60 wt % (Figure 1A-d, 0.06 g) to 0 wt % (Figure 1A-a, 0 g) causes deterioration on the structural integrity. This means that an appropriate amount of acac is favorable to maintain the ordered mesostructure. The presence of 0, 0.03, 0.045 and 0.06 g of acac results in copper contents of 0.49, 2.12, 3.32 and 5.56 wt % in the Cu_xO_y/OMC composite. In practice, an acac amount of 0.045 g is recommended to maintain the integrity of the pore structure. Figure 1B illustrates the wide-angle XRD patterns of the Cu_xO_y/OMC composite. The diffraction peaks (2θ) at 43.20°, 50.38°, 74.02° and 89.78° might be assigned to the (110), (200), (220) and (311) reflections of the cubic copper (JCPDS card 85-1326). The diffraction peaks (2θ) at 36.25° and 43.20° are consistent with the (111) and (200) reflections of CuO (JCPDS card 06-1323), and those at 36.25° and 61.45° could be attributed to the (110) and (220) reflections of Cu_2O (JCPDS card 65-3288). XRD patterns clearly indicate that the in situ grown metal nanoparticles are a well crystallized mixture of Cu, Cu_2O and CuO crystals, and thus Cu_xO_y is nominated for this mischcrystal. Additionally, a broad diffraction peak is observed within 2θ = 20−30°, which should be attributed to the amorphous carbon framework.

The XPS spectrum (Figure 2A) shows Cu $2p_{3/2}$ peak at 934.2 eV with significant shoulder peaks at 932.4.0 and 932.9 eV, showing the characteristic feature of the Cu^{II} species. In the present case, it is difficult to differentiate between Cu^0 and Cu^I states on the basis of solely XPS analysis due to the close proximity of their binding energies (ca. 932.0−933.0 eV).[24] On the other hand, TGA analysis (Figure 2B) indicates a significant weight loss is observed at a temperature <460 °C, and thereafter a stable weight is achieved due to the formation of CuO after calcination. TGA analysis derives a copper content of 3.4 wt % in the Cu_xO_y/OMC composite. This agrees well with the content achieved by ICP-MS analysis.

N_2 sorption/desorption curves in Figure 3A illustrate the typical type-IV sorption isotherms with H2 hysteresis loop for the Cu_xO_y/OMC composite. The hysteresis loop (capillary condensation) in a range of P/P_0 = 0.4−0.8 is attributed to the existence of irregular mesopores formed on the Cu_xO_y/OMC surface. The type-IV curves further indicate the presence of uniform mesopores, which is quite consistent with the feature of 2D hexagonal structure. This should be contributed to the removal of template F127 and calcination of phenolic resin framework at a high temperature.[23]

The BET surface area and pore volume of the obtained Cu_xO_y/OMC composite are calculated to be 580.8 m^2 g^{-1} and 0.64 cm^3 g^{-1}, respectively. The pore size distribution curves derived from adsorption branches using BJH model also reveal the presence of relatively uniform mesopores (Figure 3B). The mean size of the mesopore is located in the range of 4.1−6.8 nm, and the most probable aperture is ca. 5.4 nm. Similar pore structures for bare OMC are evaluated in Figure S1 (Supporting Information), where the surface area and pore size distribution for the OMC are provided, i.e., surface area of 643.5 m^2 g^{-1} and pore size centering at 5.0 nm. There is a slight decrease on the pore size for OMC with respect to Cu_xO_y/OMC (5.0 nm versus 5.4 nm); meanwhile, an increase for the surface area for bare OMC is observed with respect to Cu_xO_y/OMC (643.5 m^2 g^{-1} versus 580.8 m^2 g^{-1}).

Figure 4 shows the HR-TEM images of the Cu_xO_y/OMC composite, where oriented and hexagonally arranged pores are clearly observed, and the domain of pore size is estimated to be 5.0−8.0 nm. These results demonstrate that well-crystallized Cu_xO_y nanoparticles are highly dispersed within the ordered and hexagonally arranged pore walls in large domains without aggregation (inset).

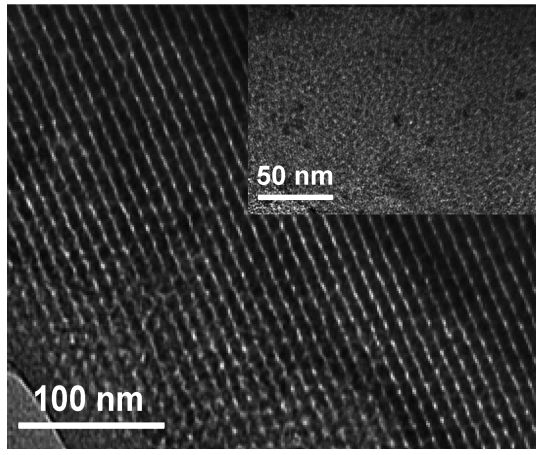

Figure 4. HR-TEM images of the Cu_xO_y/OMC composite. The inset exhibits the distribution of copper oxide nanoparticles.

Protein Adsorption Behavior of the Cu_xO_y/OMC Composite. Generally, the driving forces for the adsorption of protein species onto metal-immobilized affinity adsorbents include specific interactions, e.g., affinity binding, and non-specific interactions, e.g., electrostatic and hydrophobic interactions.[25] In the present case, all these interactions should be taken into consideration in the evaluation of protein

DOI: 10.1021/am508836m
ACS Appl. Mater. Interfaces 2015, 7, 5116−5123

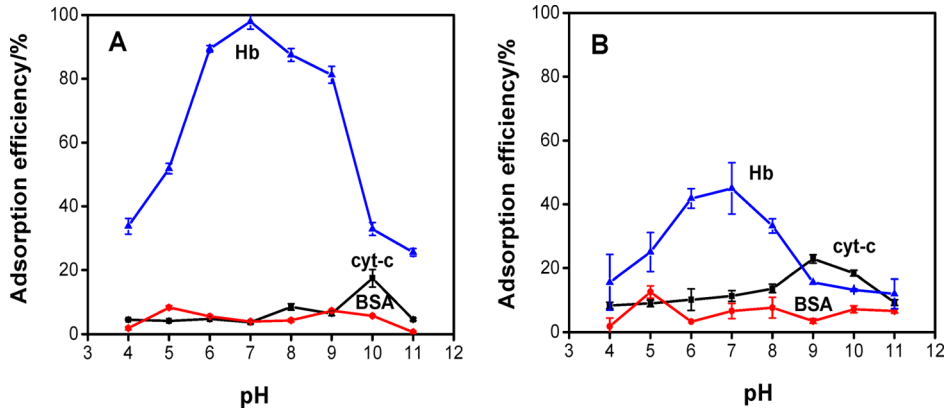

Figure 5. pH dependent adsorption behaviors of BSA, Hb and cyt-c onto the surface of Cu_xO_y/OMC composite (A) and bare OMC (B). 50 mg L^{-1} of protein in a 1.0 mL of aqueous solution is treated for 30 min with 2.0 mg of Cu_xO_y/OMC composite.

adsorption behaviors onto the Cu_xO_y/OMC composite. Surface charge analysis reveals that the Cu_xO_y/OMC composite is negatively charged within pH 4−11 (Figure S2, Supporting Information). Our experiments have demonstrated that when protein species of interest turns to positively charged, no favorable adsorption is observed. This indicated that electrostatic interactions are out of the main driving forces for the adsorption of proteins onto the Cu_xO_y/OMC composite.

Figure 5A illustrates the pH dependent adsorption of BSA, Hb and cyt-c onto the Cu_xO_y/OMC composite within a wide pH range. It is obvious that a maximum adsorption efficiency is achieved at pH value close to the isoelectric point (pI) of a specific protein species, i.e., pH 5.0 for BSA, pH 7.0 for Hb and pH 10.0 for cyt-c (it is noticed that the adsorption for BSA and cyt-c is negligible). As pH value becomes close to the isoelectric point, the protein species become neutral, which facilitates the exposure of hydrophobic residues in the protein structure. Thus, hydrophobic interaction between the Cu_xO_y/OMC composite and the protein species promotes the adsorption of the latter one. Figure 5B shows the adsorption behaviors of protein species onto bare OMC without embedded Cu_xO_y nanoparticles. It indicates similar adsorption behaviors for the three proteins as observed for the Cu_xO_y/OMC composite, i.e., favorable adsorption of proteins are achieved at their isoelectric points. These results clearly indicated that hydrophobic interaction contributes greatly to the adsorption of proteins by the copper-oxide nanoparticles embedded mesoporous carbon composite.

It should be emphasized that a much higher adsorption efficiency of hemoglobin is achieved by the Cu_xO_y/OMC composite with respect to that by bare OMC. Based on the BET analysis, the pore size of both Cu_xO_y/OMC and OMC provide sufficient entrance for the accommodation of Hb molecules. In other words, the relatively low adsorption capability by bare OMC is not due to the small pore size. In fact, the higher adsorption capacity of Cu_xO_y/OMC might be contributed to the metal-affinity interaction between the embedded Cu_xO_y nanoparticles and the histidine residues of protein. The exposure of hydrophobic residues in a neutral medium facilitates well the metal-affinity interaction, which not only provides better adsorption efficiency but also improves adsorption selectivity for Hb. In the Hb framework, there are twenty four surface exposed histidine residues,[26] while there are only two for BSA and one for cyt-c.[27] Therefore, the extensive metal-affinity interaction results in much higher adsorption for Hb, while minimum adsorption is obtained for BSA and cyt-c. To provide further elucidation in this regard, further experiments for the adsorption of hemoglobin with Cu_xO_y/OMC of similar mesostructures containing various amount of Cu (0−5.56 wt %) have been conducted at pH 7, as illustrated in Figure S3 (Supporting Information). The adsorption efficiency of hemoglobin by Cu_xO_y/OMC increases with the increase of Cu content. This indicates a dominative specific affinity interaction between the metal particles and the protein species.

On the other hand, the size of mesopore in the framework of Cu_xO_y/OMC composite distributes in the range of 4.1−6.8 nm, which is smaller than the size of BSA molecule, while larger than Hb and cyt-c. Therefore, BSA is not accessible to the mesopores of Cu_xO_y/OMC composite due to size-exclusion effect. This contributes further to the improvement on the adsorption selectivity for Hb, in combination with the previously discussed metal-affinity interaction.

The effect of ionic strength on the adsorption of protein species by the Cu_xO_y/OMC composite is investigated by the addition of certain amount of NaCl (Figure 6). The increase of ionic strength poses virtually no effect on the adsorption of the three protein species. That is to say no control of ionic strength is required in the adsorption of proteins. This observation not only further demonstrates that electrostatic interaction is not

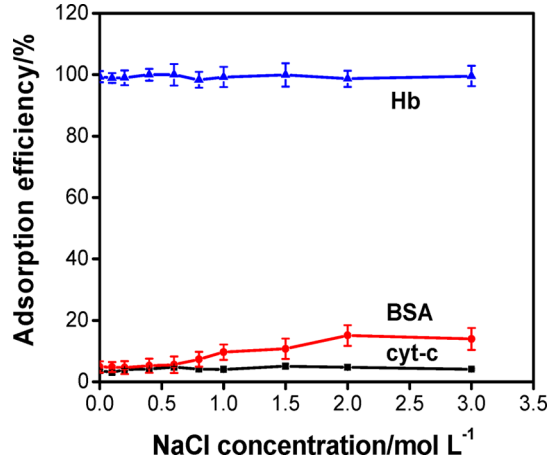

Figure 6. Dependence of protein adsorption on the variation of ionic strength within a range of 0−3 mol L^{-1} NaCl. 50 mg L^{-1} of protein in a 1.0 mL of aqueous solution (pH 7) is treated for 30 min with 2.0 mg of Cu_xO_y/OMC composite.

DOI: 10.1021/am508836m
ACS Appl. Mater. Interfaces 2015, 7, 5116−5123

among the governing driving forces for the adsorption of protein species onto the Cu_xO_y/OMC composite surface, but it also provides vast potentials of the Cu_xO_y/OMC composite for direct handling of real biological sample matrixes for the selective adsorption/isolation of hemoglobin.

The above results clearly indicated that selective adsorption of a particular protein species could be achieved by regulating pH value of the sample solution. The selective isolation of Hb in the presence of BSA and cyt-c could be readily achieved by controlling the acidity of the sample solution at pH 7, resulting in an adsorption efficiency of ca. 100% for Hb; meanwhile, virtually no adsorption is observed for BSA and cyt-c.

Figure S4 (Supporting Information) illustrates the dynamic adsorption isotherm of Hb onto the Cu_xO_y/OMC composite at room temperature within 50−5000 mg L^{-1}. It fits with Langmuir adsorption model as expressed in the following equation. C_e (mg L^{-1}) is protein concentration, Q^* (mg g^{-1}) denotes the amount of adsorbed protein at equilibrium, Q_m (mg g^{-1}) is the adsorption capacity and K_d is the dissociation constant. By fitting the experimental data to Langmuir adsorption model, a sorption capacity of 1666.7 mg g^{-1} is derived, which agrees with the actual adsorption capacity of 1482.7 mg g^{-1}.

$$Q^* = \frac{Q_m \times C_e}{k_d + C_e}$$

Table S1 (Supporting Information) compares the maximum adsorption capacity of the Cu_xO_y/OMC composite for hemoglobin with some other adsorbents. The Cu_xO_y/OMC composite offers a much higher adsorption capacity for hemoglobin. This might partially contributed by the ultrahigh specific surface area of mesoporous carbon, which provides abundant hydrophobic binding sites for the adsorption of hemoglobin. Meanwhile, the embedded copper-oxide nanoparticles in the mesopores further facilitate specific binding of Hb through metal-affinity interaction due to the large amount of histidine residues in the hemoglobin structure.

Recovery of the Adsorbed Hb from Cu_xO_y/OMC Composite. For practical biological studies, it is important to recover the adsorbed proteins from the adsorbent and transfer them into an appropriate aqueous solution. In this respect, various potential stripping reagents have been investigated for the elution of hemoglobin from the Cu_xO_y/OMC composite, including glycine−HCl, carbonate, histidine−NaOH, phosphate, BR buffer, citrate, Tris−HCl and SDS. The results in Figure S5 (Supporting Information) indicate that favorable recovery of Hb could be achieved when SDS is employed. Figure S6 (Supporting Information) shows the effect of SDS concentration on the recovery of Hb, where a recovery of 71.8% is achieved with a SDS solution of 0.5 wt %.

To evaluate the effect of the Cu_xO_y/OMC composite on the secondary structure and the biological activity of hemoglobin during the adsorption/desorption process, circular dichroism (CD) spectra are recorded for both recovered Hb by 0.5 wt % SDS and Hb standard solution prepared in a same solution. Figure 7 illustrates negative absorptions in the far UV region at 222 and 208 nm for Hb standard. This is typical feature of the predominant α-helical structure contributing to $n-\pi^*$ transfer for the peptide bond within α-helix.[28] A similar CD spectrum is obtained for the recovered Hb, indicating the maintainance of its structure with predominant α-helix.

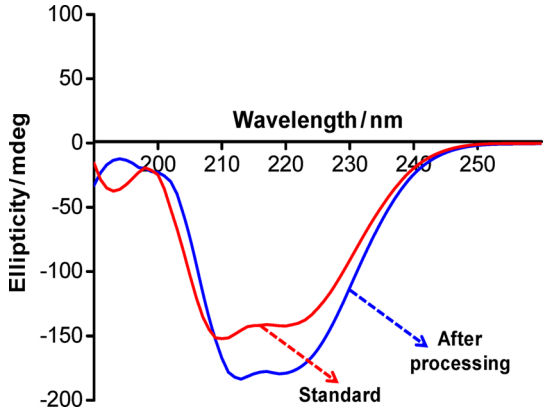

Figure 7. CD spectra of hemoglobin standard solution and that after processing by the Cu_xO_y/OMC composite and recovered in 0.5 wt % SDS solution.

The content of α-helix of Hb can be calculated according to the following equations:[29]

$$\mathrm{MRE} = \frac{\text{observed CD}}{C_p \times n \times l \times 10}$$

$$\alpha\text{-helix}\ (\%) = \frac{-\mathrm{MRE}_{208} - 4000}{33000 - 40000} \times 100$$

MRE (deg·cm^2/dmol) represents the average residue ellipticity, C_p (mol L^{-1}) denotes the protein concerntration and l is the optical path. The experimental results indicate α-helix contents of 54.84% and 54.69% for the recovered Hb and its standard solution, respectively. This observation illustrates favorable biocompatibility of the Cu_xO_y/OMC composite, which poses virtually no effect on the secondary structure of Hb during its adsorption and ensuing elution with a dilute SDS solution. To provide further elucidation on the biocompatibility of Cu_xO_y/OMC composite, comparison experiments have been done to measure the activity of standard hemoglobin in 0.5 wt % SDS and hemoglobin recovered from Cu_xO_y/OMC composite. Hemoglobin catalyzes the oxidation of 2-methoxyphenol by hydrogen peroxide, which forms a color product with a maximum absorption at 470 nm. The activity of hemoglobin is derived via the formation rate of the product, which is proportional to the oxidation rate of guaiacol.[30] The results have shown that in comparison with a standard solution of hemoglobin in 0.5 wt % SDS, 95.2% biological activity is maintained for hemoglobin recovered from the Cu_xO_y/OMC composites after adsorption. This observation in combination with the result of CD spectral analysis well demonstrated the favorable biocompatibility of the Cu_xO_y/OMC composite.

The reusability of the Cu_xO_y /OMC composite has been evaluated for the repetitive adsorption/desorption of hemoglobin, as illustrated in Figure S7 (Supporting Information). It is seen that the adsorption efficiencies for five successive adsorption processes remain virtually unchanged.

Hb Isolation from Human Blood by the Cu_xO_y/OMC Composite. The practical applicability of Cu_xO_y/OMC composite in the selective adsorption of protein is demonstrated by the isolation of hemoglobin from a complex biological sample matrix, human whole blood. The blood sample is diluted for 100-fold with 4.0 mmol L^{-1} BR buffer (pH 7) followed by centrifugation at 5000 rpm for 5 min. The supernatant is then collected to perform solid phase extraction

DOI: 10.1021/am508836m
ACS Appl. Mater. Interfaces 2015, 7, 5116−5123

with the Cu_xO_y/OMC composite, as described in the Experimental section. The retained hemoglobin is recovered from the adsorbent with elution by a 0.5 wt % SDS solution. A standard sodium dodecyl sulfate polyacrylamide gel electrophoresis (SDS-PAGE) assay[31] is afterward performed to evaluate the efficiency of the entire separation process.

The protein aqueous solutions or blood samples are first mixed with the loading buffer (a mixture of 250 mmol L^{-1} Tris−HCl (pH 6.8), 10% (w/v) SDS, 0.5% (w/v) bromophenol blue, 50% (v/v) glycerine and 5% (w/v) b-mercaptoethanol). The mixture is boiled for 5 min and then subject to electrophoresis. SDS-PAGE is carried out on a vertical polyacrylamide gel system at a constant voltage of 90 V until the protein bands reach the interface between the stacking and separating gels. The obtained electrophotogram is illustrated in Figure 8. The diluted human whole blood exhibits a few major

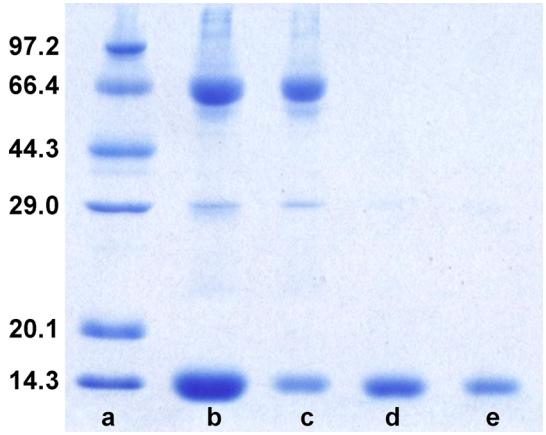

Figure 8. SDS-PAGE assay results. (a) Molecular weight standards (markers are in kDa); (b) 100-fold diluted human whole blood without pretreatment; (c) 100-fold diluted human whole blood after adsorption by the Cu_xO_y/OMC composite; (d) Hb recovered from the Cu_xO_y/OMC composite by 0.5 wt % SDS; (e) 500 mg L^{-1} Hb standard solution.

bands within a range of molecular weight from 14.3 to 66.4 kDa (lane b), attributed mainly to albumin and heme proteins including Hb. After treatment by the Cu_xO_y/OMC composite, these protein bands are still there, but the intensity for that of Hb in the effluent is greatly decreased due to its adsorption (lane c). After a 0.5 wt % SDS solution is used for stripping, the bands for other proteins are completely eliminated, leaving a clean band for Hb (lane d). This indicates high purity for the recovered Hb solution.

CONCLUSIONS

We demonstrate the fabrication of a novel copper-oxide incorporated mesoporous carbon composite, possessing a high BET surface area and large pore volume. This composite offers multimode interactions with proteins, including hydrophobic interaction, specific metal-affinity interaction between Cu_xO_y nanoparticles and the histidine residues of protein, and size-exclusion effect of the mesopores. The combination of these interactions provides an ultrahigh adsorption capacity and a favorable selectivity toward hemoglobin. The present study demonstrates the great potential of metal-doping ordered mesoporous carbon matrix in sample pretreatment, especially for the isolation or removal of specific protein species from biological samples.

ASSOCIATED CONTENT

Supporting Information

SAXS of the bare ordered mesoporous carbon and N_2 sorption/desorption isotherms and the corresponding pore size distribution curve (inset) of the bare OMC, ζ-potentials of the Cu_xO_y/OMC composite at pH 4−11, the copper content-dependent adsorption behavior of Hb onto the Cu_xO_y/OMC composite with various amount of copper, the adsorption isotherm of Hb on Cu_xO_y/OMC composite in a solution containing 4.0 mmol L^{-1} BR buffer at pH 7 and plot of $1/Q^*_{eq}$ against $1/C^*_{eq}$, the recovery of adsorbed protein (hemoglobin) from the Cu_xO_y/OMC composite with various stripping reagents, the dependence of elution efficiency of the adsorbed hemoglobin on the concentration of SDS, and the reusability efficiency of Cu_xO_y/OMC in the protein adsorption/desorption cycles. This material is available free of charge via the Internet at http://pubs.acs.org/.

AUTHOR INFORMATION

Corresponding Authors

*X.-W. Chen. E-mail: chenxuwei@mail.neu.edu.cn. Tel: +86 24 83688944. Fax: +86 24 83676698.

*J.-H. Wang. E-mail: jianhuajrz@mail.neu.edu.cn. Tel: +86 24 83688944. Fax: +86 24 83676698.

Notes

The authors declare no competing financial interest.

ACKNOWLEDGMENTS

The authors appreciate financial support from the Natural Science Foundation of China (21275027, 21235001 and 21475017), the Program of New Century Excellent Talents in University (NCET-11-0071), the SRFDP program (20120042110020), Doctoral Scientific Foundation, Liaoning Provincial Natural Science Foundation (2014020041) and Fundamental Research Funds for the Central Universities (N140506001, N141008001, N140505003 and N130105002).

REFERENCES

(1) Gutierrez, R.; del Valle, E. M.; Martin; Galan, M. A. Immobilized Metal-Ion Affinity Chromatography: Status and Trends. *Sep. Purif. Rev.* **2007**, *36*, 71−111.

(2) Block, H.; Maertens, B.; Spriestersbach, A.; Brinker, N.; Kubicek, J.; Fabis, R.; Labahn, J.; Schafer, F. Immobilized-Metal Affinity Chromatography (IMAC): A Review. *Methods Enzymol.* **2009**, *463*, 439−473.

(3) Li, F.; Dever, B.; Zhang, H. Q.; Li, X. F.; Le, X. C. Mesoporous Materials in Peptidome Analysis. *Angew. Chem., Int. Ed.* **2012**, *51*, 3518−3519.

(4) Xiao, J. J.; Bian, X. J.; Liao, L.; Zhang, S.; Ji, C.; Liu, B. H. Nitrogen-Doped Mesoporous Graphene as a Synergistic Electrocatalyst Matrix for High-Performance Oxygen Reduction Reaction. *ACS Appl. Mater. Interfaces* **2014**, *6*, 17654−17660.

(5) You, C. P.; Xu, X.; Tian, B. Z.; Kong, J. L.; Zhao, D. Y.; Liu, B. H. Electrochemistry and Biosensing of Glucose Oxidase Based on Mesoporous Carbons with Different Spatially Ordered Dimensions. *Talanta* **2009**, *78*, 705−710.

(6) Wan, L.; Zhao, Q. F.; Zhao, P.; He, B.; Jiang, T. Y.; Zhang, Q.; Wang, S. L. Versatile Hybrid Polyethyleneimine-Mesoporous Carbon Nanoparticles for Targeted Delivery. *Carbon* **2014**, *79*, 123−134.

(7) Chakravarti, R.; Mano, A.; Iwai, H.; Aldeyab, S. S.; Kumar, R. P.; Kantam, M. L.; Vinu, A. Functionalization of Mesoporous Carbon with Superbasic MgO Nanoparticles for the Efficient Synthesis of Sulfonamides. *Chem.—Eur. J.* **2011**, *17*, 6673−6682.

DOI: 10.1021/am508836m
ACS Appl. Mater. Interfaces 2015, 7, 5116−5123

(8) Stein, A.; Wang, Z.; Fierke, M. A. Functionalization of Porous Carbon Materials with Designed Pore Architecture. *Adv. Mater.* **2009**, *21*, 265−293.
(9) Lu, A. H.; Nitz, J. J.; Comotti, M.; Weidenthaler, C.; Schlichte, K.; Lehmann, C. W.; Terasaki, O.; Schüth, F. Spatially and Size Selective Synthesis of Fe-based Nanoparticles on Ordered Mesoporous Supports as Highly Active and Stable Catalysts for Ammonia Decomposition. *J. Am. Chem. Soc.* **2010**, *132*, 14152−14162.
(10) Wang, W.; Wang, H. Y.; Wei, W.; Xiao, Z. G.; Wan, Y. Self-Assembling and Size-Selective Synthesis of Ni and NiO Nanoparticles Embedded in Ordered Mesoporous Carbon and Polymer Frameworks. *Chem.—Eur. J.* **2011**, *17*, 13461−13472.
(11) Sietsma, J. R.; Meeldijk, J. D.; den Breejen, J. P.; Versluijs-Helder, M.; van Dillen, A. J.; de Jongh, P. E.; de Jong, K. P. The Preparation of Supported NiO and Co_3O_4 Nanoparticles by the Nitric Oxide Controlled Thermal Decomposition of Nitrates. *Angew. Chem., Int. Ed.* **2007**, *119*, 4631−4633.
(12) Ryoo, R.; Joo, S. H.; Kruk, M.; Jaroniec, M. Ordered Mesoporous Carbons. *Adv. Mater.* **2001**, *113*, 677−681.
(13) Lee, J.; Kim, J.; Hyeon, T. Recent Progress in the Synthesis of Porous Carbon Materials. *Adv. Mater.* **2006**, *18*, 2073−2094.
(14) Kruk, M.; Jaroniec, M.; Kim, T. W.; Ryoo, R. Synthesis and Characterization of Hexagonally Ordered Carbon Nanopipes. *Chem. Mater.* **2003**, *15*, 2815−2823.
(15) Vinu, A.; Hossian, K. Z.; Srinivasu, P.; Miyahara, M.; Anandan, S.; Gokulakrishnan, N.; Mori, T.; Ariga, K.; Balasubramanian, V. V. Carboxy-Mesoporous Carbon and Its Excellent Adsorption Capability for Proteins. *J. Mater. Chem.* **2007**, *17*, 1819−1825.
(16) Yu, T.; Deng, Y. H.; Wang, L.; Liu, R. L.; Zhang, L. J.; Tu, B.; Zhao, D. Y. Ordered Mesoporous Nanocrystalline Titanium-Carbide/Carbon Composites from in Situ Carbothermal Reduction. *Adv. Mater.* **2007**, *19*, 2301−2306.
(17) Gao, W.; Wan, Y.; Dou, Y.; Zhao, D. Y. Synthesis of Partially Graphitic Ordered Mesoporous Carbons with High Surface Areas. *Adv. Energy Mater.* **2011**, *1*, 115−123.
(18) Meng, Y.; Gu, D.; Zhang, F.; Shi, Y.; Yang, H.; Li, Z.; Yu, C.; Tu, B.; Zhao, D. Y. Ordered Mesoporous Polymers and Homologous Carbon Frameworks: Amphiphilic Surfactant Templating and Direct Transformation. *Angew. Chem., Int. Ed.* **2005**, *44*, 7053−7059.
(19) Zhai, Y. P.; Dou, Y. Q.; Liu, X. X.; Park, S. S.; Ha, C. S.; Zhao, D. Y. Soft-Template Synthesis of Ordered Mesoporous Carbon/Nanoparticle Nickel Composites with a High Surface Area. *Carbon* **2011**, *49*, 545−555.
(20) Sun, Z. K.; Sun, B.; Qiao, M. H.; Wei, J.; Yue, Q.; Wang, C.; Deng, Y. H.; Kaliaguine, S.; Zhao, D. Y. A General Chelate-Assisted Co-assembly to Metallic Nanoparticles-Incorporated Ordered Mesoporous Carbon Catalysts for Fischer−Tropsch Synthesis. *J. Am. Chem. Soc.* **2012**, *134*, 17653−17660.
(21) Zhang, M.; Wu, Y. P.; Feng, X. Z.; He, X. W.; Chen, L. X.; Zhang, Y. K. Fabrication of Mesoporous Silica-Coated CNTs and Application in Size-Selective Protein Separation. *J. Mater. Chem.* **2010**, *20*, 5835−5842.
(22) Liu, J. W.; Zhang, Q.; Chen, X. W.; Wang, J. H. Surface Assembly of Graphene Oxide Nanosheets on SiO_2 Particles for the Selective Isolation of Hemoglobin. *Chem.—Eur. J.* **2011**, *17*, 4864−4870.
(23) Gao, P.; Wang, A. Q.; Wang, X. D.; Zhang, T. Synthesis of Highly Ordered Ir-Containing Mesoporous Carbon Materials by Organic-Organic Self-Assembly. *Chem. Mater.* **2008**, *20*, 1881−1888.
(24) NIST X-ray Photoelectron Spectroscopy Database, http://srdata.nist.gov/xps/.
(25) Qian, K.; Wan, J. J.; Liu, F.; Girault, H. H.; Liu, B. H.; Yu, C. Z. A Phospho-directed Macroporous Alumina-Silica Nanoreactor with Multi-functions. *ACS Nano* **2009**, *3*, 3656−3662.
(26) Wuenschell, G. E.; Naranjo, E.; Arnold, F. H. Pasadena. Aqueous Two-Phase Metal Affinity Extraction of Heme Proteins. *Bioprocess Biosyst. Eng.* **1990**, *5*, 199−202.
(27) Ma, Z. Y.; Liu, X. Q.; Guan, Y. P.; Liu, H. Z. Synthesis of Magnetic Silica Nanospheres with Metal Ligands and Application in Affinity Separation of Proteins. *Colloids Surf., A* **2006**, *275*, 87−91.
(28) Xie, X. Y.; Wang, X. R.; Xu, X. M.; Sun, H. J.; Chen, X. G. Investigation of the Interaction between Endocrine Disruptor Bisphenol A and Human Serum Albumin. *Chemosphere* **2010**, *80*, 1075−1080.
(29) Guo, X.; Han, X.; Tong, J.; Guo, C.; Yang, W.; Zhu, J.; Fu, B. The Investigation of the Interaction between Piracetam and Bovine Serum Albumin by Spectroscopic Methods. *J. Mol. Struct.* **2010**, *966*, 129−135.
(30) Shu, Y.; Chen, X. W.; Wang, J. H. Ionic Liquid-Polyvinyl Chloride Ionomer for Highly Selective Isolation of Basic Proteins. *Talanta* **2010**, *81*, 637−642.
(31) Laemmli, U. K. Cleavage of Structural Proteins during the Assembly of the Head of Bacteriophage T4. *Nature* **1970**, *227*, 680−685.

DOI: 10.1021/am508836m
ACS Appl. Mater. Interfaces 2015, 7, 5116−5123